Article

Seismic Benefits of a Vibrating Mass Equipped with an Inerter on Frame Structures Due to Soil Interaction

Angelo Di Egidio [1],[*],[†] and Alessandro Contento [2],[†]

1   Dipartimento di Ingegneria Civile, Edile-Architettura e Ambientale (DICEAA), University of L'Aquila, 67100 Poggio di Roio, Italy
2   College of Civil Engineering, Fuzhou University, Fuzhou 350025, China; alessandro@fzu.edu.cn
*   Correspondence: angelo.diegidio@univaq.it
†   These authors contributed equally to this work.

Abstract: The reduction of the seismic effects on new and existing structures is a relevant topic of the structural mechanics applied to the civil engineering. Usually, the conceptual aspects related to a new approach are studied by means of low-dimensional mechanical models able to capture the main dynamic aspects of the method. The present paper can be framed in this context. Specifically, the paper investigates the possibility of reducing the seismic response of a frame structure by using a vibrating mass connected to an inerter device, which interacts through the soil to protect the structure. The problem is studied by using existing soil–structure interaction (SSI) and structure–soil–structure interaction (SSSI) models, which describe the actions between the structure and the soil, and among adjacent structures through linear visco-elastic devices. A seven-degrees-of-freedom mechanical model is used to describe the problem, where a general multi-story frame structure is mathematically described by means of an equivalent 2-degrees-of-freedom system. The external vibrating mass is coupled with the inerter device to increase its inertia without using high real mass. The aim of the paper is to point out the role of the many parameters that characterize the interaction system. Particular attention is devoted to the mechanical characteristics of the soil, in order to know the effectiveness of the SSSI system as a function of the characteristics of the soil. Results show that the vibrating mass equipped with the inerter device is almost always beneficial for the frame structure to be protected. However, sufficient good performances justifying the costs of this method can be reached only in limited ranges of the characterizing parameters.

Keywords: structure–soil–structure interaction; vibrating mass; inerter device; frame structure; seismic behavior

1. Introduction

The seismic protection of new or existing structures stands as a cornerstone within the field of Civil Engineering. Numerous possibilities exists for the preliminary assessment of the effectiveness of new protection techniques. When a proposed technique aims to influence the behaviour of an entire structure rather than focusing on local interventions, one viable approach involves evaluating its effectiveness using a simplified archetype mechanical model. This initial step yields insights that warrant more exhaustive analyses employing refined models, despite their higher computational costs. The present paper seamlessly fits into this narrative, employing an archetypal model to explore the feasibility of implementing a cutting-edge seismic protection system for frame structures.

The use of low-dimensional models to explore methods for mitigating seismic responses in structures has been extensive. Within scholarly literature, two-degrees-of-freedom (2-DOF) models have been often employed to study the conceptual aspects related to seismic protection methodologies. For instance, comprehensive studies on Base Isolation (BI) have been conducted in [1], while investigations into Tuned Mass Damper (TMD)

systems have been detailed in [2]. These simplified models have also facilitated the analysis of various modifications and combinations of these techniques. Notably, Tsai [3] and Taniguchi et al. [4] delved into the reduction of base displacement in base-isolated systems through the integration of TMDs. Recently, the same objective has been pursued in [5,6] using TMDIs, i.e., combinations of TMDs and inerter devices. The effectiveness of such devices in controlling seismic responses has also been investigated using low-dimensional mechanical models, as demonstrated in [7,8].

More complex low-dimensional mechanical models have been recently employed to investigate the seismic protection of frame structures by coupling them with external systems. Noteworthy, a Hysteretic Mass Damper Inerter (HMDI) [9] and an external elastic structure equipped with an inerter [10] have been used as coupled external systems to enhance the seismic response of frame structures.

The prevailing trend observed in numerous papers, including those aforementioned, is the direct attachment of external systems to the target structure for protection. However, recent studies have investigated the prospect of enhancing structural response by considering the interaction mediated through the soil between an external system and the structure under consideration. In essence, this entails a scenario where the structure and the external system are not directly coupled but interact indirectly through the soil medium.

The topic of structure–soil–structure interaction (SSSI) provides the tools to model interactions among different structures through the soil medium. The use of vibrating masses or barriers, enhanced with inerter devices, interacting through the soil with a target structure for sesimic protection, requires the application of SSSI models found in the scientific literature. In [11], a comprehensive review of the state of the art in recent papers addressing the SSSI problem is presented. In [12–14], researchers investigated the use of vibrating masses or barriers equipped with inerter devices, to improve the seismic response of structures, and the interaction between the vibrating mass and the structure was modeled using existing SSSI models.

The analysis method applied in this paper is similar to that in [13,14], where a low-dimensional model was used to describe the structure–soil–structure interaction between the vibrating mass and the structure to be protected, both represented by one-dimensional systems, with only the soil's horizontal dynamics considered. These studies pioneered the concept of mitigating seismic responses in structures by leveraging soil interaction with an external system. In alignment with this approach, the present paper shares a similar objective and employs a low-dimensional model to represent structure–soil–structure interaction. Specifically, it investigates reducing seismic responses in frame structures by utilizing soil interaction with a vibrating mass equipped with an inerter device. In this paper, a mechanical type of inerter device, designed to exert a force that is directly proportional to the relative acceleration between two connection points, or terminals, is considered. A common design approach involves using a rack-pinion-flywheel assembly [15,16]. It is pertinent to clarify that this paper does not aim to refine existing soil–structure interaction (SSI) and structure–soil–structure interaction (SSSI) models. Instead, these models serve as indispensable tools for modeling the interaction between structures and the soil, as well as between adjacent structures. Specifically, the models employed in this study characterize the soil utilizing linear viscoelastic Kelvin–Voigt devices, with their damping and stiffness properties derived from specific relationships. For further elucidation on the utilized SSI and SSSI models, readers are directed to Section 2.2.

Compared to [13,14], the original contributions primarily pertain to the following aspects:

- The rotational motion of a portion of soil is accounted for, leading to a dual level of interaction between structures and the soil.
- The structure to be protected is a frame structure and is modeled using a 2-DOF dynamically equivalent system. Employing a 2-DOF model, rather than a simpler 1-DOF system, enables the capture of additional information on the behavior of the structure.

- The parametric analysis extends to parameters defining the soil properties beneath both the protected structure and the external system (comprising the vibrating mass and inerter device). This comprehensive approach allows for the consideration of soil heterogeneity across different locations.
- The visualization of parametric results through performance maps, constructed by varying the characteristics of the vibrating mass and inerter, facilitates the identification of optimal parameter ranges where the system exhibits superior effectiveness.

The system under investigation comprises two foundation platforms. One of these platforms supports the vibrating mass, which is connected to the platform via a viscoelastic device and to an inerter device [17]; consequently, the two terminals of the inerter are linked with the vibrating mass and directly with the ground. Positioned atop the second platform is the frame structure intended for protection. Both the horizontal displacements and rotations of the platforms, along with the horizontal displacement of the vibrating mass, are considered Lagrangian parameters. Conversely, the multi-story frame structure to be protected is modeled using a 2-degree-of-freedom equivalent system, employing two Lagrangian parameters. Hence, to describe the interaction system, a seven-degree-of-freedom mechanical system is employed.

Two distinct series of parametric analyses are undertaken. The initial series involves the systematic variation of the stiffness of the device linking the vibrating mass to the foundation platform and the virtual mass provided by the inerter device. The results are presented in performance maps, which illustrate the performance metrics across the parameter space. These metrics are the ratios between two specific displacements of the structure interacting with the vibrating mass and the corresponding displacements of the standalone structure, i.e., the structure without the seismic protection system. The two displacements are that of the first-story drift and the total drift of the structure. The second series of parametric analyses explores the influence on the dynamics of the structure of parameters characterizing the soil and certain geometrical characteristics of the foundation platforms. Such influence is analyzed by examining the alterations in specific sections of the performance maps resulting from variations in the aforementioned parameters.

2. Mechanical Model

As outlined in the introduction, the primary objective of this investigation is to assess the feasibility of enhancing the seismic performances of frame structures through the integration of a vibrating mass coupled with an inerter device, which interacts with the frame via the soil medium (Figure 1). The problem under investigation can be categorized within the domain of SSI and SSSI. Oftentimes, models used for SSI and SSSI assume that the soil–structure and inter-structural interactions can be described by suitable equivalent linear dash-pots and elastic springs [18,19]. In this paper, an established model of SSSI, widely accepted within the scientific community, is employed [20]. Particular attention is devoted to assess the sensitivity of the dynamics of the protected structure to the geometrical and mechanical parameters that characterize such an SSSI model.

2.1. Model of the Frame Structure Connected to Vibrating Mass and an Inerter Device

The SSSI problem is investigated using a low-dimensional mechanical model designed to capture the fundamental dynamics of the actual structure. This low-dimensional model, termed the archetype model (see Figure 2a), comprises two primary components: (i) the external system acting as a protection device and (ii) the system to be protected against earthquakes.

The external system consists of a foundation platform with a mass m_e, upon which is situated the vibrating mass M_r interacting with the inerter device having a virtual mass M_I (referred to as inertance). Withing the external system, the parameters k_M and c_M define the linear elastic connection between the vibrating mass M_r and the foundation platform.
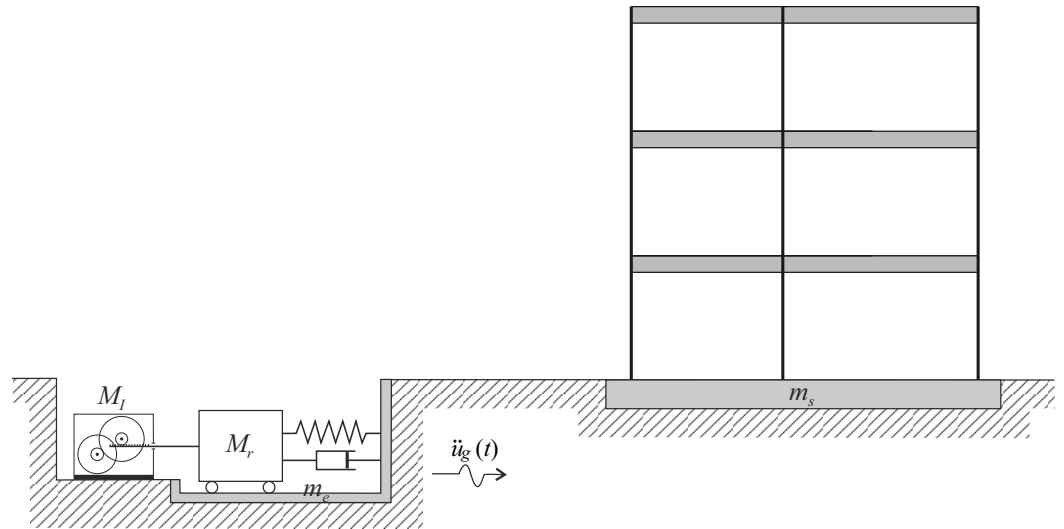
Figure 1. Interaction through the soil between vibrating mass with inerter and frame structure.

The system to be seismically protected consists of a foundation platform with a mass m_s supporting the frame structure. The multi-degree-of-freedom (M-DOF) structure is represented by a dynamically equivalent 2-degree-of-freedom (2-DOF) shear-type model with masses m_1 and m_2. The definition of such equivalent 2-DOF model exploits the dynamic equivalence proposed in [21,22]. This dynamic equivalence provides the mass m_i, stiffness k_i, and damping c_i ($i = \{1,2\}$) associated with each of the two degrees of freedom. More specifically, the 2-DOF equivalent system is constructed such that the degree of freedom associated with m_1 models the displacement of the first story of the real M-DOF frame structure, whereas the second degree of freedom associated with m_2 models the displacement of the final story of the real structure.

The connection between the two platforms and the soil is represented by Kelvin–Voigt devices characterized by linear and rotational stiffness coefficients k_j and $k_{\theta j}$, along with the corresponding damping coefficients c_j and $c_{\theta j}$, where $j = \{e, s\}$. Subscript $j = e$ denotes parameters pertaining to the external platform, whereas those with subscript $j = s$ pertain to the platform supporting the frame structure. Additionally, the interaction between the external system and the frame structure occurring through the soil is modeled through an additional Kelvin–Voigt device characterized by the four coefficients k_{es}, $k_{\theta es}$, c_{es}, and $c_{\theta es}$. The two coefficients with subscript θ refer to rotational components of the Kelvin–Voigt devices, essential for capturing the rotational dynamics of the two platforms. However, for the sake of simplicity, these rotational components are omitted from the graphical representation in Figure 2a.

Overall, the archetype system is described by seven Lagrangian parameters, whose positive directions are shown in Figure 2b. Specifically, u_j and θ_j, where $j = \{e, s\}$, describe the displaced configuration of the two foundation platforms, whereas u_M, u_1, and u_2 are the relative displacements of the vibrating mass M_r and the 2-DOF equivalent frame system with respect to the corresponding foundation platforms.

The equations of motion are derived through a Lagrangian approach. The displacement components of the masses defining the system, expressed as functions of the Lagrangian parameters according to Equation (1):

$$
\begin{aligned}
x_e(t) &= u_e(t) + u_g(t), \\
x_{M_r}(t) &= u_e(t) + u_M(t) - \theta_e(t)h_e + u_g(t), \\
x_s(t) &= u_s(t) + u_g(t), \\
x_1(t) &= u_s(t) + u_1(t) - \theta_s(t)h_1 + u_g(t), \\
x_2(t) &= u_s(t) + u_2(t) - \theta_s(t)h_2 + u_g(t).
\end{aligned}
\tag{1}
$$

Such displacements are needed to write the kinetic energy possessed by the system according to Equation (2):

$$
\begin{aligned}
T = {} & \frac{1}{2}(I_e + I_M)\dot{\theta}_e^2(t) + \frac{1}{2}(I_s + I_1 + I_2)\dot{\theta}_s^2(t) + \frac{1}{2}m_e\dot{x}_e^2(t) + \frac{1}{2}M_r\dot{x}_{M_r}^2(t) + \\
& \frac{1}{2}M_I\dot{x}_{M_I}^2(t) + \frac{1}{2}m_s\dot{x}_s^2(t) + \frac{1}{2}m_1\dot{x}_1^2(t) + \frac{1}{2}m_2\dot{x}_2^2(t),
\end{aligned}
\tag{2}
$$

where $\dot{x}_{M_i}(t) = \dot{u}_e(t) + \dot{u}_M(t) - \dot{\theta}_e(t)h_e$ represents the relative velocity between the two terminals of the inerter device, characterized by the virtual mass M_I, the quantities I_e and I_s denote the polar inertia of the foundation platforms, and their masses, m_e and m_i, also account for the virtual contribution of the soil below the platforms. The explicit definition of these four quantities is provided in Section 2.2. The polar inertia of the oscillating mass (I_M) and the two stories of the 2-DOF equivalent system $(I_1$ and $I_2)$ are deemed negligible $(I_M = I_1 = I_2 = 0)$. The potential energy, needed to apply the Lagrangian approach, reads based on Equation (3):

$$
\begin{aligned}
U = {} & \frac{1}{2}k_e u_e(t)^2 + \frac{1}{2}k_s u_s(t)^2 + \frac{1}{2}k_{\theta e}\theta_e(t)^2 + \frac{1}{2}k_{\theta s}\theta_s(t)^2 + \frac{1}{2}k_M u_M(t)^2 + \\
& \frac{1}{2}k_1 u_1(t)^2 + \frac{1}{2}k_2(u_2(t) - u_1(t))^2 + \frac{1}{2}k_{es}(u_s(t) - u_e(t))^2 + \frac{1}{2}k_{\theta es}(\theta_s(t) - \theta_e(t))^2,
\end{aligned}
\tag{3}
$$

where the stiffness of the Kelvin–Voigt devices representing the soil are defined in Section 2.2. Furthermore, to take into account the viscous non-conservative forces, the effect of such forces has to be considered. This effect, denoted as W, is formulated according to Equation (4):

$$
\begin{aligned}
W = {} & -[c_e\dot{u}_e(t)u_e(t) + c_s\dot{u}_s(t)u_s(t) + c_{\theta e}\dot{\theta}_e(t)\theta_e(t) + c_{\theta s}\dot{\theta}_s(t)\theta_s(t) + c_M\dot{u}_M(t)u_M(t) + \\
& c_1\dot{u}_1(t)u_1(t) + c_2(\dot{u}_2(t) - \dot{u}_1(t))(u_2(t) - u_1(t)) + c_{es}(\dot{u}_s(t) - \dot{u}_e(t))(u_s(t) - u_e(t)) + \\
& c_{\theta es}(\dot{\theta}_s(t) - \dot{\theta}_e(t))(\theta_s(t) - \theta_e(t))],
\end{aligned}
\tag{4}
$$

where, c_1, c_2, and c_M are the damping coefficients that refer to the 2-DOF system and the oscillating mass. The other coefficients provide the viscous damping of the Kelvin–Voigt devices representing the soil and are defined in Section 2.2.

By introducing the Lagrangian function $L = T - U$ and letting $\{q_1, q_2, q_3, q_4, q_5, q_6, q_7\} = \{u_e, \theta_e, u_M, u_s, \theta_s, u_1, u_2\}$, the seven Lagrangian equations of motion are obtained according to Equation (5):

$$
\left[\frac{\delta}{\delta t}\left(\frac{\delta L}{\delta \dot{q}_i}\right) - \frac{\delta U}{\delta q_i} - \frac{\delta W}{\delta q_i}\right]dq_i = 0, \quad \forall dq_i \neq 0, \quad (i = 1, \ldots, 7).
\tag{5}
$$

Such equations of motion read based on Equation (6):

$$
\begin{aligned}
& m_e(\ddot{u}_e + \ddot{u}_g) + M_R(\ddot{u}_e + \ddot{u}_M - \ddot{\theta}_e h_e + \ddot{u}_g) + M_I(\ddot{u}_e + \ddot{u}_M - \ddot{\theta}_e h_e) + \\
& c_e u_e - c_{es}(\dot{u}_s - \dot{u}_e) + k_e u_e - k_{es}(u_s - u_e) = 0, \\
& (I_e + I_M)\ddot{\theta}_e - M_R(\ddot{u}_e + \ddot{u}_M - \ddot{\theta}_e h_e + \ddot{u}_g)h_e - M_I(\ddot{u}_e + \ddot{u}_M - \ddot{\theta}_e h_e)h_e + \\
& c_{\theta e}\dot{\theta}_e - c_{\theta es}(\dot{\theta}_s - \dot{\theta}_e) + k_{\theta e}\theta_e - c_{\theta es}(\theta_s - \theta_e) = 0, \\
& M_R(\ddot{u}_e + \ddot{u}_M - \ddot{\theta}_e h_e + \ddot{u}_g) + M_I(\ddot{u}_e + \ddot{u}_M - \ddot{\theta}_e h_e) + c_M\dot{u}_M + k_M u_M = 0, \\
& m_s(\ddot{u}_s + \ddot{u}_g) + m_1(\ddot{u}_s + \ddot{u}_1 - \ddot{\theta}_s h_1 + \ddot{u}_g) + m_2(\ddot{u}_s + \ddot{u}_2 - \ddot{\theta}_s h_2 + \ddot{u}_g) + \\
& c_s\dot{u}_s + c_{es}(\dot{u}_s - \dot{u}_e) + k_s u_s + k_{es}(u_s - u_e) = 0, \\
& (I_s + I_1 + I_2)\ddot{\theta}_s - m_1(\ddot{u}_s + \ddot{u}_1 - \ddot{\theta}_s h_1 + \ddot{u}_g)h_1 - m_2(\ddot{u}_s + \ddot{u}_2 - \ddot{\theta}_s h_2 + \ddot{u}_g)h_2 + \\
& c_{\theta s}\dot{\theta}_s + c_{\theta es}(\dot{\theta}_s - \dot{\theta}_e) + k_{\theta s}\theta_s + k_{\theta es}(\theta_s - \theta_e) = 0, \\
& m_1(\ddot{u}_s + \ddot{u}_1 - \ddot{\theta}_s h_1 + \ddot{u}_g) + c_{11}\dot{u}_1 + c_{12}\dot{u}_2 + k_1 u_1 - k_2(u_2 - u_1) = 0, \\
& m_2(\ddot{u}_s + \ddot{u}_2 - \ddot{\theta}_s h_2 + \ddot{u}_g) + c_{21}\dot{u}_1 + c_{22}\dot{u}_2 - k_2 u_1 + k_2 u_2 = 0.
\end{aligned}
\tag{6}
$$

It worth observing that, contrarily to the oscillating mass M_r, the virtual mass of the inerter device M_I responds only to the relative acceleration between its two terminals, $\ddot{u}_e + \ddot{u}_M - \ddot{\theta}_e h_e$. As a consequence, the external seismic acceleration $\ddot{x}_g$ does not influence the virtual mass M_I as it does to the real mass M_r. In Equation (6), c_{ij}, where $\{i, j\} = \{1, 2\}$, represents the coefficients of the symmetric Rayleigh damping matrix of the standalone frame structure on rigid soil. The Rayleigh damping matrix is obtained according to Equation (7):

$$\begin{bmatrix} c_{11} & c_{12} \\ c_{21} & c_{22} \end{bmatrix} = \alpha \begin{bmatrix} m_1 & 0 \\ 0 & m_2 \end{bmatrix} + \beta \begin{bmatrix} k_1 + k_2 & -k_2 \\ -k_2 & k_2 \end{bmatrix}, \tag{7}$$

where coefficients α and β are derived under the assumption of identical relative damping coefficients for both modes of the standalone frame structure, denoted by $\xi = 0.05$. Finally, the damping c_M is determined by modeling the moving mass M as a 1-DOF system with a relative damping of $\xi_M = 0.05$. Specifically, $c_M = 2M\xi_M\omega_M$, where $\omega_M = \sqrt{k_M/M}$ and $M = M_r + M_I$.
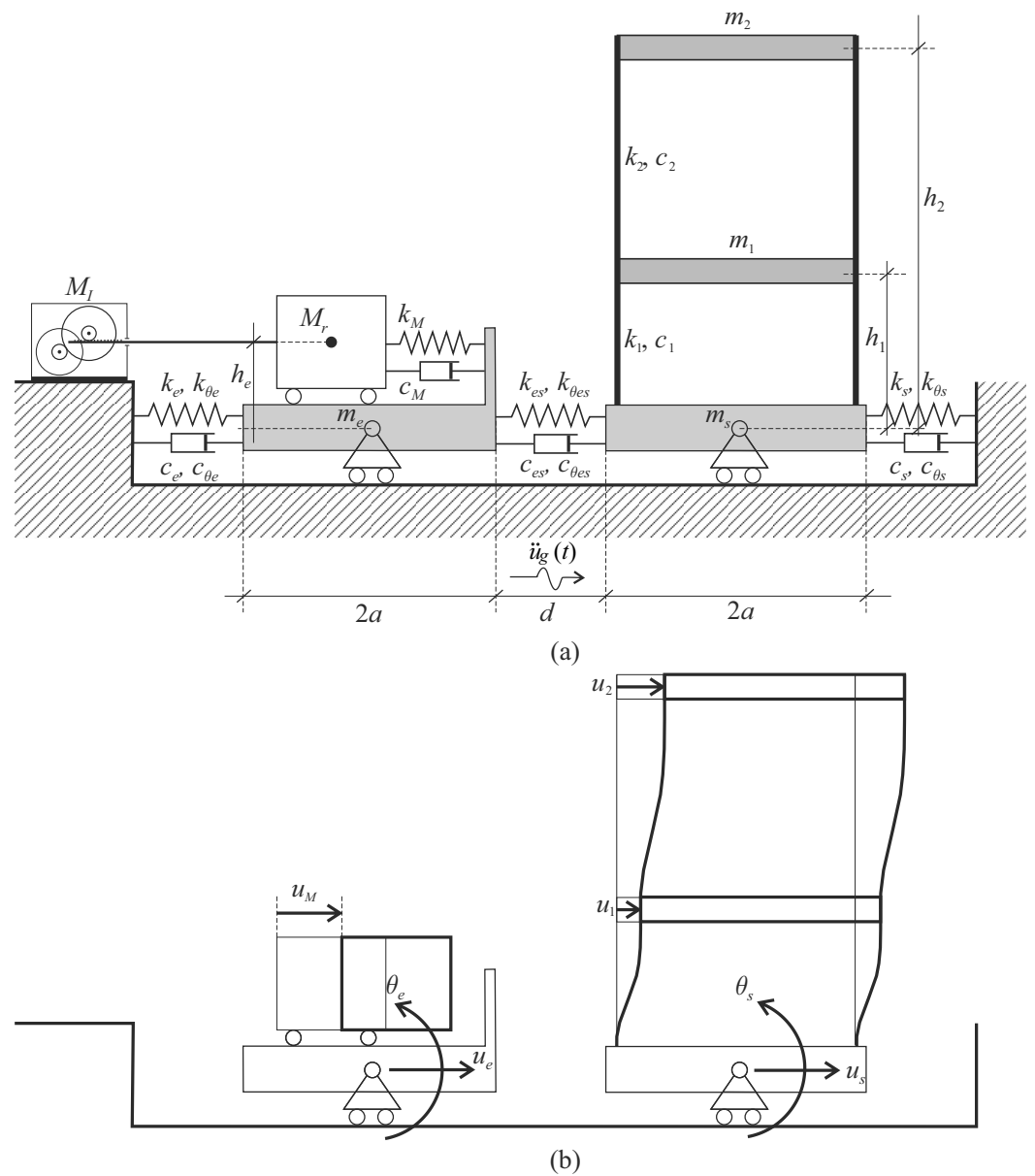

Figure 2. Archetype low-dimensional mechanical model. (**a**) Geometrical and mechanical characteristics of the system. (**b**) Positive Lagrangian parameters.

2.2. Structure–Soil–Structure Interaction Model

The SSSI model used in the present paper is borrowed from [20]. This model is a simplification of the comprehensive model derived in [18,19]. A notable simplification concerns the dimensions of the foundation platforms. Specifically, in the model proposed in [20], the platforms are assumed to be square-shaped with equal sides of length $2a$ (see Figure 2).

Given the equivalence in the dimensions of the foundation platforms, their masses and polar inertia coincide ($m_s = m_e$ and $I_s = I_e$). These parameters are adjusted to incorporate contributions from the underlying soil. To derive such quantities, virtual contributions attributable to the soil (m_{ve}, m_{vs}, I_{ve}, and I_{vs}) are added to the initial masses ($m_{fe} = m_{fs}$) and polar moments of inertia ($I_{fe} = I_{fs}$) of the foundation platforms. Specifically, the total mass m_e and the total polar inertia I_e are determined according to Equation (8):

$$
\begin{aligned}
m_e &= m_{fe} + m_{ve}, \\
I_e &= I_{fe} + I_{ve}.
\end{aligned}
\tag{8}
$$

The initial mass m_{fe} and polar moment of inertia I_{fe} only depend on the geometrical and mechanical properties of the foundation platforms, and thus, they are known quantities, defined according to Equation (9):

$$
\begin{aligned}
m_{fe} &= 2a \times 2a \times t \times \rho_p, \\
I_{fe} &= m_{fe} \times \left[\frac{t^2}{12} + \frac{(2a)^2}{12} \right],
\end{aligned}
\tag{9}
$$

where t and ρ_p are the thickness and mass density of the foundation platform, respectively. The virtual contributions (m_{ve} and I_{ve}) are provided as fractional proportions of m_{fe} and I_{fe} and are formulated according to Equation (10):

$$
\begin{aligned}
mv_e &= \frac{0.095 m_{fe}}{\beta_e}; \quad \beta_e = \frac{(1 - \nu_{max}) m_{fe}}{4 \rho r_0^3}; \\
Iv_e &= \frac{0.095 I_{fe}}{\beta_{\theta e}}; \quad \beta_{\theta e} = \frac{3(1 - \nu_{max}) m_{fe}}{8 \rho r_0^5};
\end{aligned}
\tag{10}
$$

where $r_0 = 2a \big/ (3\pi)^{1/4}$ and ρ is the mass density of the soil.

In accordance with [20], the stiffness and damping coefficients of the Kelvin–Voigt devices used to model the interaction between the two foundation platforms and the soil, illustrated in Figure 2, are specified based on Equation (11):

$$
\begin{aligned}
k_e &= \chi \frac{9.2 G_{max} a}{2 - \nu_{max}}; \quad k_{\theta e} = \chi \frac{4.0 G_{max} a^3}{1 - \nu_{max}}; \quad c_e = \frac{0.163 a}{V_s} k_e; \quad c_{\theta e} = \frac{0.6a}{V_s} k_{\theta e} \\
k_s &= \frac{9.2 G_{max} a}{2 - \nu_{max}}; \quad k_{\theta s} = \frac{4.0 G_{max} a^3}{1 - \nu_{max}}; \quad c_s = \frac{0.163 a}{V_s} k_s; \quad c_{\theta s} = \frac{0.6a}{V_s} k_{\theta s}.
\end{aligned}
\tag{11}
$$

Moreover, the stiffness and damping of the devices decribing the structure–soil–structure interaction (see Figure 2) are defined according to Equation (12):

$$
\begin{aligned}
k_{es} &= \left[3.7561 \times 10^{-0.18995\left(\frac{d}{a}\right)} \right] \frac{G_{max} a}{2 - \nu_{max}}; \quad k_{\theta es} = -\left(0.04234 - 0.2396 \mathrm{Log}\left(\frac{d}{a}\right) \right) \frac{G_{max} a^3}{1 - \nu_{max}} \\
c_{es} &= 13.2875 \frac{G_{max} a^2}{V_s(2 - \nu_{max})}; \quad c_{\theta es} = \left(7.3823 - 6.775 \mathrm{Log}\left(\frac{d}{a}\right) \right) \frac{G_{max} a^4}{V_s(1 - \nu_{max})};
\end{aligned}
\tag{12}
$$

where $G_{max} = V_s^2 \rho$ is the maximum shear modulus of the soil under small strains, V_s is the shear wave velocity, and ν_{max} the Poisson coefficient of the soil under small strains.

The parameters referring to the external system, k_e and $k_{\theta e}$, are scaled by a factor $\chi \leqslant 1$. Such factor is introduced to model the effect of the application of Geotechnical Seimic Isolation (GSI) [23,24] to the external system. In general, the application of the GSI produces a reduction of the stiffness of the soil. It is worth remarking that the paper does not refer to a specific GSI model, but aims to investigate the role of the soil characteristics below the external protection device, simply scaling the stiffness of the soil. Although the application of the GSI also modifies the damping of the soil, in this paper, this aspect is not taken into account. As can be observed in Equation (12), the stiffness and the damping depend on the ratio d/a, where d is the distance between the two foundation platforms and $2a$ is the dimension of such platforms (see Figure 2).

Finally, it is important to highlight the assumptions used to build the model, which may limit the investigation of actual structural systems. Specifically:

- The interaction between the foundation platforms and the soil, as well as between the two structures through the soil, is studied by modeling the soil with linear Kelvin–Voigt devices. Although commonly used in SSSI problems, this assumption considers the soil as functioning in both tension and compression.
- The adopted SSSI model assumes equal dimensions for the foundation platforms, a hypothesis that may be difficult to prove in practical applications. However, since this paper presents a preliminary parametric study based on the use of simplified mechanical models, its aim is to offer general insights into this approach rather than specific design guidelines.
- Using a low-dimensional mechanical model that captures only the primary dynamics of actual structures provides preliminary insights into the effectiveness of this protection method. For the application to real structures, a more comprehensive analysis should be performed.
- The inerter device is assumed to be connected to an infinitely stiff soil and to the vibrating mass. This assumption would require the use of a deep foundation to connect the inerter to the bedrock, ensuring that one of its terminals directly experiences the earthquake acceleration.

3. Definition of the Characteristics of the System Used in the Analyses

To examine the efficacy of the interaction between the external protection device and a frame structure through the soil, an in-depth parametric analysis is conducted. Among all the parameters that influence the dynamic behavior of the SSSI system, this section clarifies which parameters are considered the most relevant for this study and, consequently, treated as variables, and which are held constant throughout the analyses. While this approach focuses on the most relevant parameters, further insights could be gained by varying some of the parameters currently fixed. Expanding the set of variable parameters presents a compelling direction for future studies where a specific tuning of the protection method is needed to address specific case studies.

3.1. Variable Parameters

The variable parameters under consideration encompass the characteristics of the external protection device, the SSSI model, the soil, and the frame structures. Specifically, they include:

- The stiffness k_M and the virtual mass M_I provided by the inerter device. These two mechanical quantities are parameterized in relation to the stiffness k_1 and the mass m_1 of the 2-DOF model associated with the degree of freedom u_1, according to Equation (13):

$$
\begin{aligned}
k_M &= \eta k_1, \\
M_I &= \gamma m_1.
\end{aligned}
\tag{13}
$$

- The ratio between the distances d and a, the shear wave velocity V_s of the soil, and the scaling coefficient χ (see Equation (11)). For clarity, the ratio d/a that appears explicitly in Equation (12) has been renamed introducing the parameter α, as defined in Equation (14):

$$\alpha = \frac{d}{a}. \tag{14}$$

- The characteristics of the frame structure. Two distinct structures are considered in the analyses. It is assumed that these structures are sufficiently regular to be effectively modeled by M-DOF shear-type systems. Furthermore, equal mass and stiffness distribution are considered at each story. The main characteristics of the two systems are presented in Table 1.

Table 1. Geometrical and mechanical characteristics of the two reference frame structures.

	Stories	Area [m^2]	Mass [kg]	Stiffness [Nm^{-1}]	Height [m]	Period [s]	2a [m]
Frame 1	4	250	301.5×10^3	4.22×10^8	3.0	0.48	16.0
Frame 2	5	350	422.1×10^3	6.29×10^8	3.0	0.57	19.0

Table 1 presents the number of stories for each structure, as well as the area, mass, stiffness, and height assigned to each story. Additionally, Table 1 includes the main vibration period of the structure (Period) and the base dimension of the square foundation platforms $2a$. Table 2 displays the geometrical and mechanical quantities that characterize the 2-DOF systems (refer to Figure 2). The heights h_1 and h_2 provide the vertical position of the mass centers associates to the two DOF (i.e., the mass of the first story and the lumped mass of all of the other stories) with respect to the mass center of the foundation platform. Specifically, since the first level of the equivalent 2-DOF system always corresponds to the first story of the actual frame structure, h_1 is the height of the first story. The height h_2 of the second level represents the vertical position of the center of mass of all the stories above the first.

Table 2. Mechanical characteristics of the 2-DOF equivalent systems.

	k_1 [Nm^{-1}]	k_2 [Nm^{-1}]	m_1 [kg]	m_2 [kg]	h_1 [m]	h_2 [m]
Frame 1	7.93×10^8	2.44×10^8	301.5×10^3	904.5×10^3	3.50	9.50
Frame 2	1.07×10^9	2.55×10^8	422.1×10^3	1688.4×10^3	3.50	11.0

3.2. Fixed Quantities

Certain parameters, deemed less significant for variation, are consistently held constant throughout the paper. Specifically, these parameters include:

- Thickness of the two foundation platforms, $t = 0.5$ m;
- Mass density of the material of the foundation platforms, $\rho_p = 2400$ kg/m^3;
- Height from the foundation platform of the mass center of the vibrating mass, $h_e = 1.5$ m;
- Mass density of the soil, $\rho = 2100$ kg/m^3;
- Poisson coefficient of the soil at small strains, $\nu_{max} = 1/3$;
- Vibrating mass, $M_r = m_1$.

4. Parametric Analysis

An initial parametric analysis is performed by varying the parameters that characterize the components of the SSSI system.

4.1. Earthquake Records

Three earthquake records are used as excitation. The selection of these records considers differences in their spectral characteristics. The number of records is limited because the intention is to qualitatively assess the sensitivity of the protection method to the characteristics of the earthquake record, rather than to provide a specific design methodology for the protection system. Figure 3 presents the time histories of the selected records (Figure 3a) and their corresponding pseudo-acceleration elastic spectra (Figure 3b).

The following earthquake records are considered in this study:

(a) El Centro, 1940 California, Array Sta 9, Imperial Valley Irrigation District, 302 Commercial, component 180, position of the station: 32.7953 N, 115.5335 W;

(b) Kobe, 1995 Japan earthquake, Takarazuka station, 0 deg, ground level, position of the station: 34.8090 N, 135.3440 W;

(c) San Jose, 1989 Fremont Mission San Jose motion, Loma Prieta earthquake, California USA.

For clarity, each record is denoted by its corresponding underlined name from this list. The earthquake records were obtained from the 'Center for Engineering Strong Motion Data' [25].

It is worth observing that, due to the linearity of the model, the fundamental aspect that characterizes the response of the mechanical system is closely related to the frequency content of the seismic excitation.
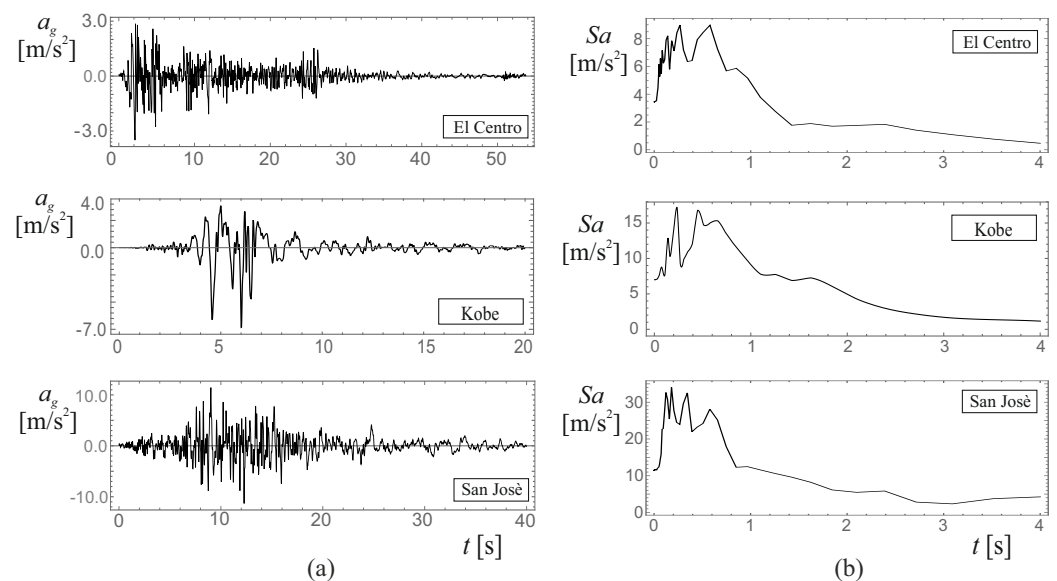

Figure 3. Records of El Centro, Kobe, and San Josè seimic events. (**a**) Time history. (**b**) Pseudo-acceleration spectrum (based on [25]).

4.2. The Role of the Parameters Characterizing the Vibrating Mass with Inerter

The first analysis is performed by varying k_M and mass M_I through η and γ (see Equation (13)), while maintaining the constants $V_s = 500$ m/s, $\alpha = 1.0$, and $\chi = 1.0$. This analysis focuses on evaluating the displacement u_1 and drift $\Delta u = u_2 - u_1$ of Frame 1 under the Kobe earthquake. The results are displayed as surface plots and contour maps of u_1 (Figure 4b) and Δu (Figure 4b) across the parameter space defined by γ and η. The plots elucidate a substantial dependency of the frame structure's response on both γ and μ, showcasing specific parameter combinations (or regions within the parameter space), where u_1 and Δu exhibit relative minimum values. These regions of relative minima offer valuable insights for the choice of optimal design parameters for the external device, which could lead to an effective mitigation of the structural response of the frame under seismic loading conditions.
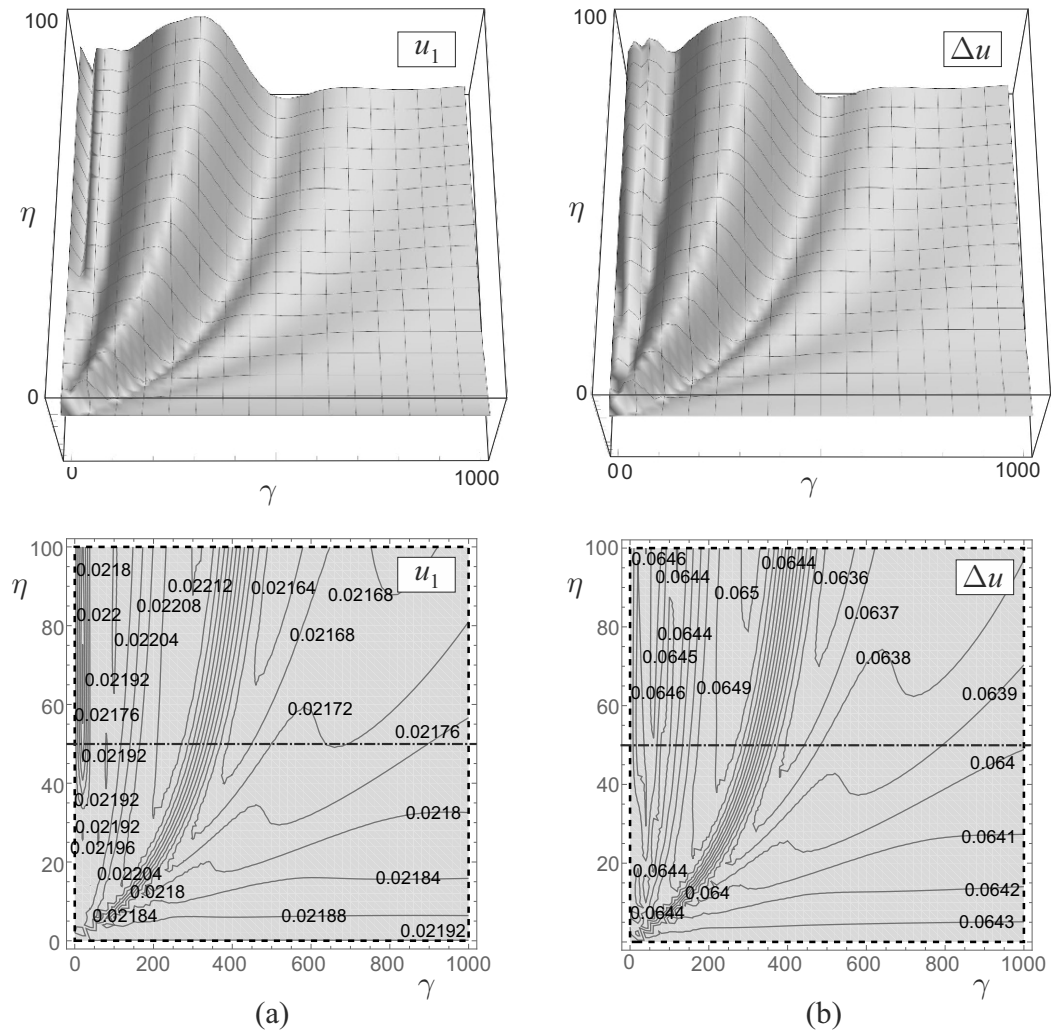
Figure 4. Displacement surfaces and maps of the 4-story frame structure under the Kobe earthquake. (**a**) Displacement u_1. (**b**) Drift Δu ($V_s = 500 \, \text{m/s}$, $\alpha = 1.0$, $\chi = 1.0$).

4.3. The Role of the Parameters Characterizing the SSSI System

In order to assess the sensitivity of the structural dynamics to the various parameters defining the SSSI (structure–soil–structure interaction) system, the response of the frame structure is analyzed with η held constant at a value of $\eta = 50$. This specific value corresponds to the sections delineated by dash-dot lines in Figure 4. Figure 5 juxtaposes these sections for u_1 (on the left) and Δu (on the right) with analogous curves derived by individually varying the remaining parameters. All the graphs of Figure 5 are represented in the same scale, facilitating a direct comparison of the impacts stemming from modifications in the different parameters. This common scale enables a concise assessment of the influence of parameter variations on the structural response, aiding in the identification of the key factors affecting the system dynamics. Figure 5a illustrates the sensitivity analysis with respect to α (refer to Equation (14)) while maintaining fixed values for $V_s = 500 \, \text{m/s}$ and $\chi = 1.0$. The bold curve corresponds to the section extracted from the surfaces depicted in Figure 4, representing the case where $\alpha = 1.0$. The results indicate that variations in the parameter α (which corresponds to the separation distance d between the two foundation platforms) have a negligible impact on the structural response of the frame, as evidenced by the close proximity of the different curves.
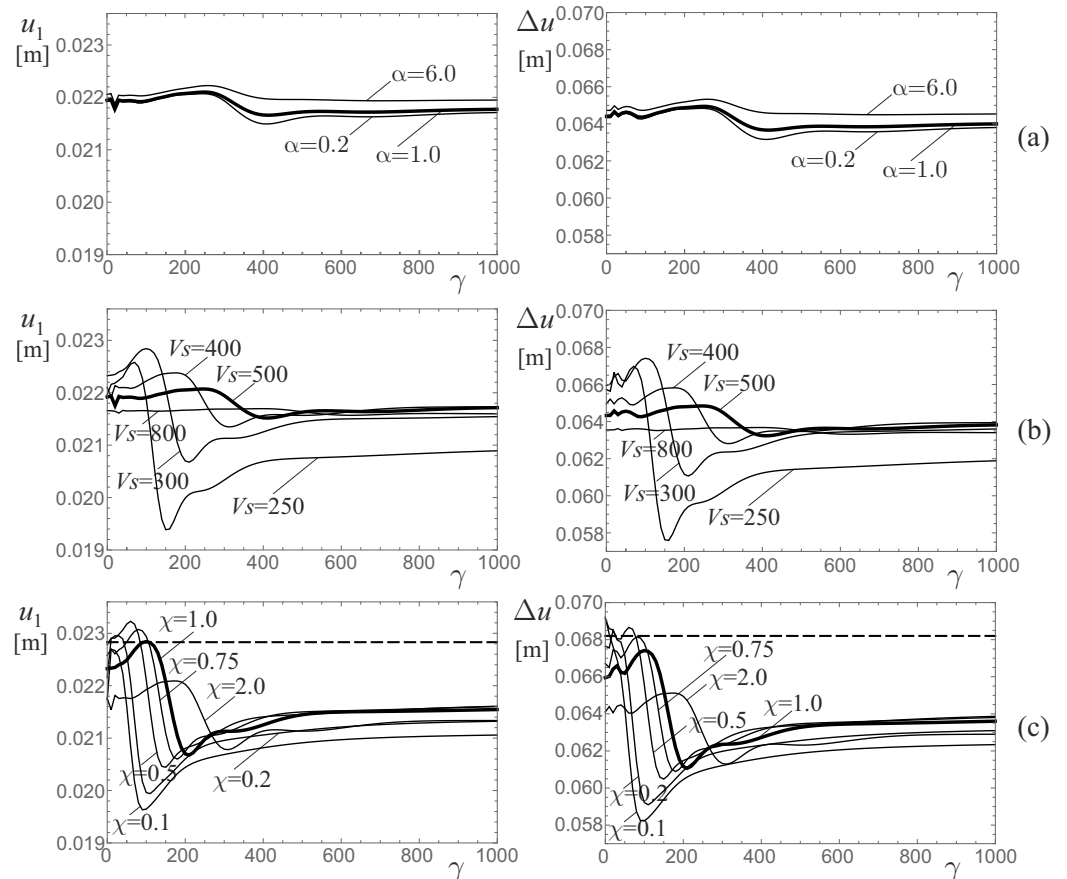
Figure 5. Section at $\eta = 50$ of the maps of the 4-story frame structure under the Kobe earthquake. (**a**) Variation of α ($V_s = 500$ m/s, $\chi = 1.0$). (**b**) Variation of V_s ($\alpha = 0.2$, $\chi = 1.0$). (**c**) Variation of χ ($\alpha = 0.2$, $V_s = 300$ m/s).

Figure 5b demonstrates the impact of the shear wave velocity V_s of the soil on the structural response. It is important to note that this analysis is not intended to alter the soil characteristics, but rather to assess the performance of the proposed interaction as a function of V_s. This approach allows for determining in advance whether the method is suitable for a specific case and soil type. The various curves in the graphs correspond to different values of V_s while maintaining fixed values for $\alpha = 0.2$ and $\chi = 1.0$. The bold curves coincide with those presented in Figure 5a, representing the case where $\alpha = 0.2$ and $V_s = 500$ m/s. Notably, the curve associated with the highest value of $V_s = 800$ m/s exhibits a nearly constant profile compared to the other curves. A decrease in the shear wave velocity V_s significantly alters the system behavior, leading to notable changes in the minimum values of both u_1 and Δu. This trend suggests improved performance of the SSSI system with lower values of V_s. However, for smaller virtual mass parameter γ, the structural response shows an increase in both displacement and drift. Nevertheless, such increments are confined to specific ranges of γ, highlighting the complex interplay between system parameters and structural behaviour.

Finally, Figure 5c investigates the influence of χ (refer to Equation (11)), which represents the reduction in the soil's stiffness beneath the foundation of the external device resulting from the implementation of the GSI (Ground Stiffness Improvement) technique. The curves in the graphs correspond to varying values of χ while maintaining fixed values for $\alpha = 0.2$ and $V_s = 300$ m/s. The bold curves align with those depicted in Figure 5b, representing the scenario with $\chi = 1$ and $V_s = 300$ m/s. Both graphs include the response of the frame structure in the absence of the external device (standalone structure); such a response, identified by the dashed straight line, accounts solely for the interaction of the structure with the soil beneath its foundation platform. The findings indicate that the mini-

mum values of both u_1 and Δu decrease as χ is reduced. Consequently, lower soil stiffness beneath the external protection system enhances the performance of the SSSI system. Furthermore, within the scope of small γ, decreasing values of χ lead to an intensified system response surpassing that of the standalone frame structure. Nevertheless, irrespective of the values of χ and γ, with a few exceptions, the response of the SSSI system consistently remains below that of the standalone structure. These results underscore the beneficial effects of reducing χ in enhancing the structural performance under seismic conditions. Additionally, they highlight the importance of considering the combined influence of χ and γ in optimizing the behavior of the SSSI system, ensuring superior performance compared to the standalone structure.

5. Seismic Performance of the SSSI System

In this section, a parametric analysis is conducted on both Frame 1 and Frame 2 (refer to Tables 1 and 2) across the range of the selected earthquakes. The analysis focuses on varying the parameters associated with the vibrating mass, namely k_M and M_I, while maintaining fixed values for $\alpha = 0.2$, $V_s = 300 \text{ m/s}$, and $\chi = 0.2$. This systematic exploration allows for a comprehensive assessment of the structural response under different seismic scenarios, providing valuable insights into the dynamic behaviour of both Frame 1 and Frame 2.

5.1. Performance Indexes and Maps

To assess the effectiveness of the SSSI system in mitigating the structural response, two performance indices are introduced according to Equation (16):

$$\alpha_1 = \frac{\max|u_1(t)|}{\max|\tilde{u}_1(t)|}, \ \alpha_2 = \frac{\max|\Delta u(t)|}{\max|\tilde{\Delta} u(t)|} \tag{15}$$

where $\tilde{u}_1$ and $\tilde{\Delta} u = \tilde{u}_1 - \tilde{u}_2$ denote the displacement and drift of the 2-degree-of-freedom (2-DOF) model representing the standalone structure. The effectiveness of the SSSI system improves as the values of α_1 and α_2 decrease relative to unity.

The parametric analysis involves mapping the values of the performance indices, α_1 and α_2, onto the parameter plane defined by η and γ using a single earthquake record. This process generates performance maps, which are contour plots illustrating the distribution of the indices α_1 and α_2 across the $\eta - \gamma$ parameter space. To enhance readability, the contour levels are delineated using a specific greyscale scheme, where lighter shades correspond to smaller values of the performance indices. Optimal performance of the SSSI system is observed within regions of the maps characterized by clearer greyscale tones. These areas indicate superior system performance, as denoted by lower values of the performance indices α_1 and α_2.

5.2. Performance Maps of the SSSI System

Figure 6 illustrates the performance maps of α_1 (left column) and α_2 (right column) for Frame 1 subjected to El Centro (top row), Kobe (middle row), and San Jose (bottom row) seismic excitations. It is noteworthy that the performance indexes across all parameter spaces are consistently below unity. Nevertheless, discernible regions within the maps exhibit enhanced performance of the SSSI system. Notably, these regions demonstrate consistent performance improvements across all three seismic events, suggesting the potential for identifying parameter values that yield robust performance regardless of the specific earthquake scenario. While this observation holds promise, its generalizability warrants further investigation through a comprehensive analysis encompassing a diverse range of seismic events. However, such an exhaustive study falls beyond the scope of the current paper. For the specified parameters ($\alpha = 0.2$, $V_s = 300 \text{ m/s}$, and $\chi = 0.2$), the SSSI system is shown to achieve a notable reduction of approximately 20% in both u_1 and Δu compared to the performance of the standalone frame structure.
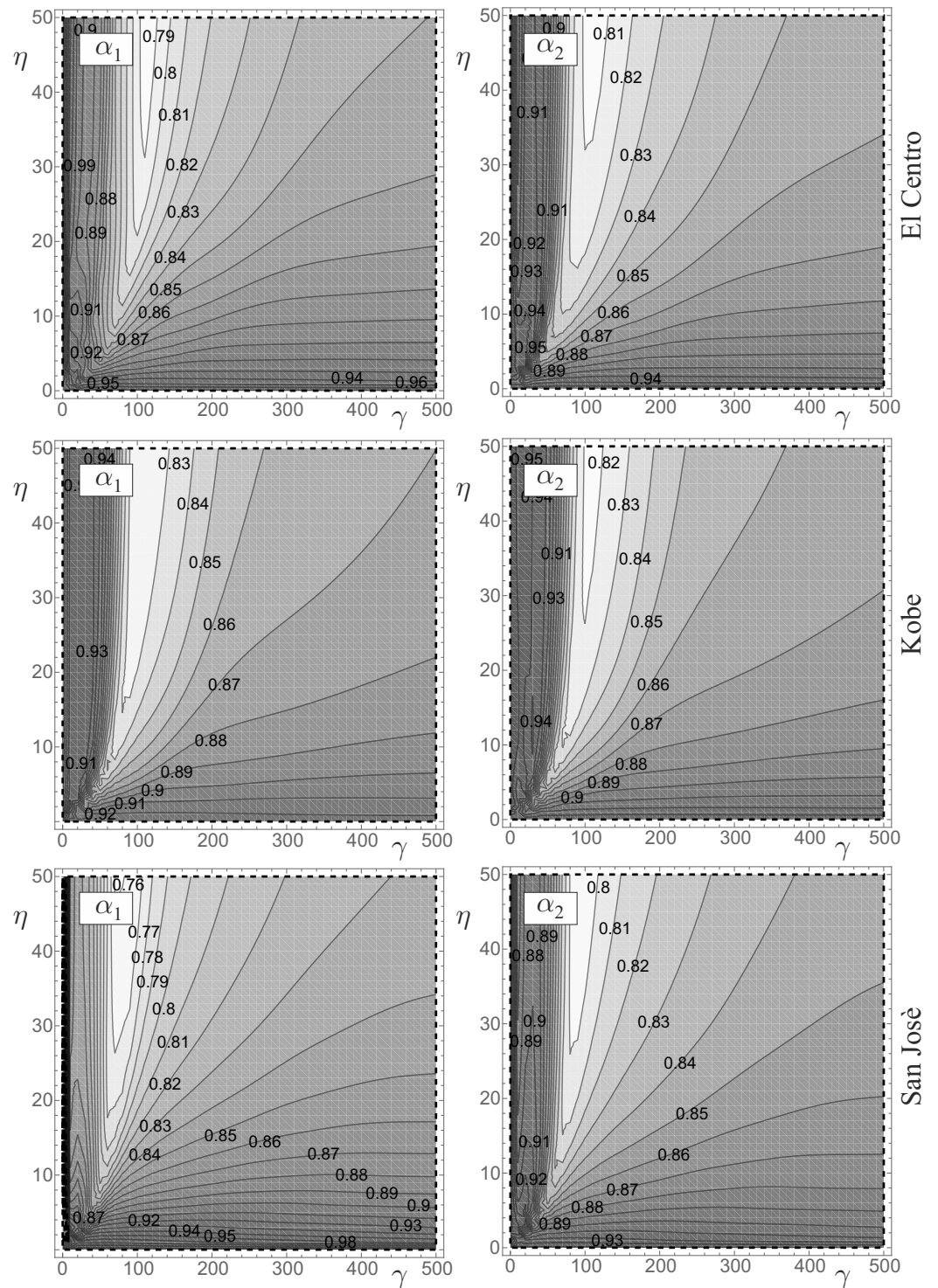
Figure 6. Performance α_1 and α_2 maps of the 4-story frame structure under several earthquakes ($\alpha = 0.2$, $V_s = 300$ m/s, $\chi = 0.2$).

Similar results are observed for Frame 2. Figure 7 is constructed similar to Figure 6 and presents the performance maps of α_1 (left column) and α_2 (right column) for Frame 2 under three selected earthquakes (El Centro in the first row, Kobe in the second, and San Jose in the third and last row). Consistently across the parameter space, the performance indexes remain below unity. Notably, distinct regions within these maps exhibit superior performance of the SSSI system. These regions demonstrate consistent performance enhancements across all three seismic scenarios, mirroring the observations made for Frame

1. However, it is worth highlighting that these performance-improving regions in Frame 2 are situated within parameter ranges different from those identified for Frame 1. This underscores the influence of the structural properties of the frame on the optimal parameter selection for ensuring the enhanced performance of the SSSI system. In essence, the identification of parameters that yield optimal SSSI system performance appears to be related to the mechanical characteristics of the frame structure being protected. In conclusion, the comparison between Frame 1 and Frame 2, considering that Frame 2 is larger than Frame 1 (consisting of 5 stories with an area of 350 m^2 compared to 4 stories with an area of 250 m^2 for Frame 1), reveals the following findings:

- Achieving optimal performance of the SSSI system with Frame 2 necessitates higher values of η and γ compared to those required for Frame 1. This highlights the influence of the structural dimensions on the parameter settings that yield effective SSSI system performance.
- The extent of reduction in u_1 and Δu, as quantified by α_1 and α_2, is comparatively lower in Frame 2 than in Frame 1. This disparity indicates that, attributable to the greater mass of Frame 2 relative to Frame 1, the SSSI system exhibits enhanced performance for the smaller Frame 1.

5.3. Spectral Analysis

This section explores the effectiveness of SSSI system in mitigating the seismic response of frame structures. Given the linearity of the mechanical system, conducting a spectral analysis becomes a logical step. Specifically, analyzing the vibration periods and modal shapes across distinct locations within the parameter space $\eta - \gamma$ can yield critical insights into the system's functionality.

Figure 8 presents the vibration periods and modal shapes of both the standalone and SSSI systems. The spectral analysis of the latter is conducted for two configurations identified by points *A* and *B* on the performance maps related to α_1 and α_2 that have been obtained for the San Jose earthquake, in Figure 7. Specifically, Figure 8a illustrates the first two vibration periods and associated modal shapes of the standalone structure. It should be emphasized that the standalone system is defined by four Lagrangian parameters (illustrated in the right section of the system in Figure 2b), thereby admitting four modes. Figure 8b,c display the initial four vibration periods and associated modal shapes of the SSSI system, which possesses a total of seven modes. The analysis deliberately concentrates on the initial modes of both systems, based on the assumption that the primary dynamic effects are predominantly influenced by these modes.

At Point *A*, both α_1 and α_2 exhibit values slightly less than unity. This point is situated in a region of the performance maps, where the effectiveness of the external protection system in reducing the response of the frame structure is comparatively lower, as indicated by the darker shade of gray. Conversely, Point *B* is located along the locus (represented by a dotted thick curve) where relative minima of the performance indices are observed. Consequently, for the selected value of $\eta = 50$, Point *B* corresponds to the optimal performance of the SSSI system, while Point *A* demonstrates the least effective performance. Independently from the chosen combination of parameters, in both *A* and *B*, the SSSI system generally exhibits higher periods for the first modes compared to the standalone system. This effect can be attributed to the substantial mass of the external protection system, which can be theoretically increased as desired through the incorporation of an inerter device. Consequently, the first modes of the SSSI system are shifted towards spectral regions where seismic activity exhibits reduced power content.
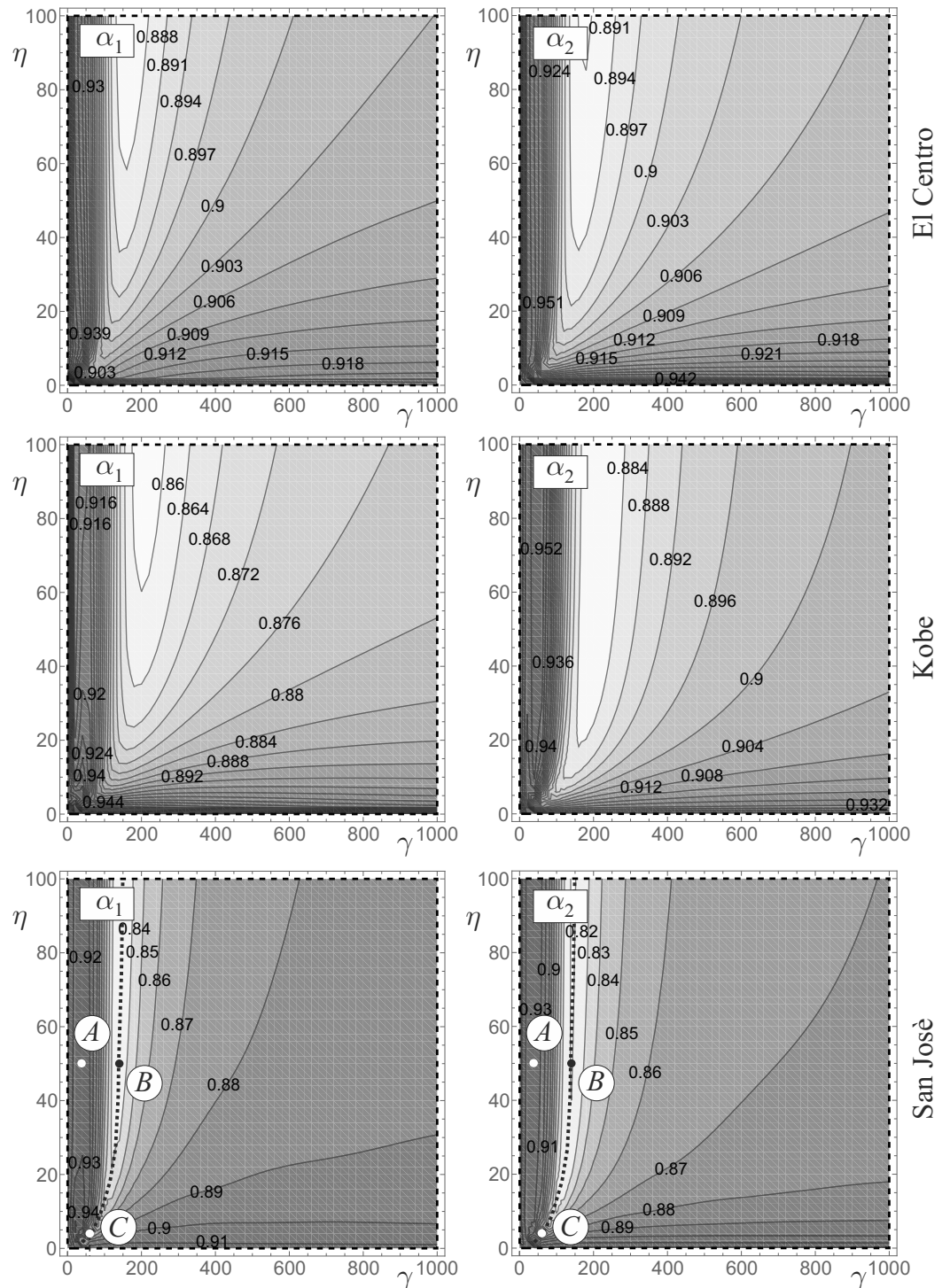
Figure 7. Performance α_1 and α_2 maps of the 5-story frame structure under several earthquakes ($\alpha = 0.2$, $V_s = 300$ m/s, $\chi = 0.2$).

The analysis of results for Point *A* (Figure 8b) reveals that the two foundation platforms consistently move in phase across all four modes. Furthermore, in the first three modes, the entire translating mass of the external protection system also moves in phase with the foundation platform of the frame structure. It is reasonable to hypothesize that the dynamic contributions from these first three modes enhance the motion intensity at the base of the frame structure. Conversely, in the fourth mode, the vibrating mass moves in counter-phase relative to the foundation platform, which may lead to an improvement in the response. It is also observed that the periods of Mode 2 and Mode 4 in the SSSI system are close to

the periods of the first two modes of the standalone structure. The modest enhancement in the response of the SSSI system compared to the standalone system, as indicated by performance index values slightly less than unity, is primarily attributable to Mode 4. In this mode, the vibrating mass moves in counter-phase relative to both foundation platforms, thereby mitigating the dynamic effects transferred to the base of the frame structure.
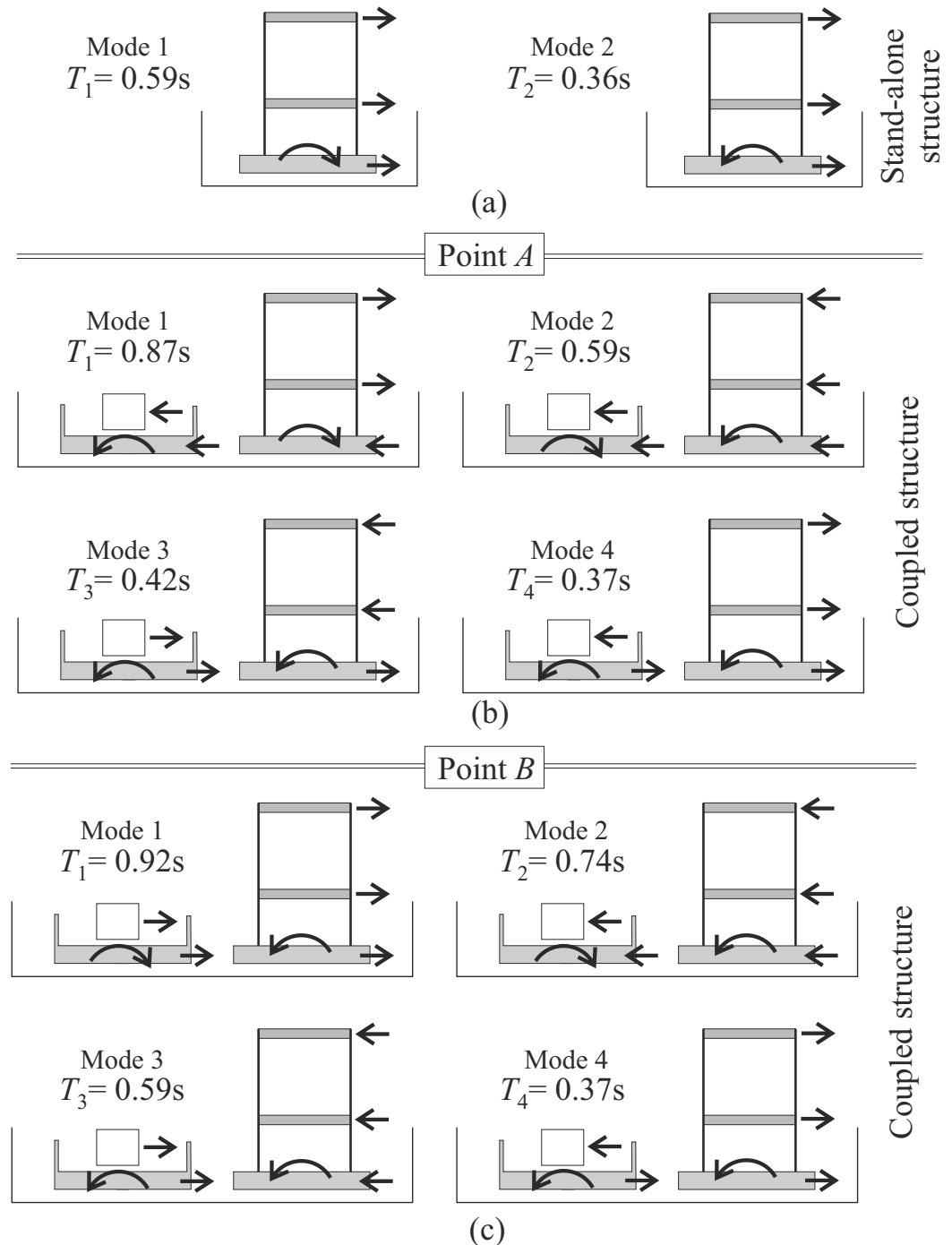

Figure 8. Periods and modal shapes of systems labeled in point *A* and *B* in Figure 7. (**a**) Standalone structure . (**b**) Point *A* ($\eta = 50$, $\gamma = 37.5$, $\alpha = 0.2$, $V_s = 300$ m/s, $\chi = 0.2$) . (**c**) Point *B* ($\eta = 50$, $\gamma = 137.5$, $\alpha = 0.2$, $V_s = 300$ m/s, $\chi = 0.2$).

Results obtained for the system designated as Point *B* (Figure 8c) indicate that the external protection system and the foundation platform of the frame structure move in phase only in the first two modes. However, these modes exhibit periods longer than the initial pe-

riod of the standalone structure, generally reducing their dynamic significance. Conversely, Modes 3 and 4, which have periods closely matching those of the standalone structure, display either total or partial movement of the external protection system in counter-phase relative to the foundation platform of the frame structure. Specifically, in Mode 3, the entire external protection system moves in counter-phase relative to the foundation platform of the frame structure, whereas in Mode 4, only the vibrating mass moves in counter-phase relative to both foundation platforms. Therefore, since Modes 3 and 4 of the SSSI system effectively replace the corresponding modes of the standalone structure due to the proximity of their periods, the benefit of the SSSI system is greater at Point *B* compared to Point *A*. This is because both the third and fourth modes contribute to a reduction in the dynamic effects transmitted to the base of the frame structure.

A further confirmation of the previous assertions can be obtained by analyzing the time histories of the SSSI system. Figure 9 shows the time histories of some referring displacement of systems characterized by parameters $\eta - \gamma$ of Point *A*, Point *B*, and Point *C* on the San Jose performance maps of Figure 7. Specifically, in Figure 9a, each graph shows the u_e and u_M components, whereas in Figure 9b, each graph shows the u_e and u_s components. Each row of Figure 9 shows graphs whose time histories refer to the three different points *A*, *B*, and *C*.

Further validation of the previous assertions is provided by the analysis of the time histories of the SSSI system. Figure 9 displays the time histories of specific displacements associated with systems characterized by parameters $\eta - \gamma$ for Points *A*, *B*, and *C* on the San Jose performance maps of Figure 7. Specifically, Figure 9a presents the time histories of the u_e and u_M displacements, while Figure 9b displays the time histories of u_e and u_s. Each row of Figure 9 corresponds to the time histories associated with one of the three distinct points *A*, *B*, and *C*.

Starting from Point *A*, the comparison of the time histories for the displacements u_e and u_M indicates that the displacement of the vibrating mass u_M is significantly smaller than that of the foundation platform of the external protection system u_e. Additionally, these two displacements are substantially in phase with each other. The comparison between displacements u_e and u_s also shows that these two components are in phase, corroborating the results from the spectral analysis which indicated that in almost all modal shapes at Point *A*, the components of the two foundation platforms are in phase. Consequently, the benefits of the external protection system in mitigating seismic effects on the frame structure are minimal, as reflected by the proximity of α_1 and α_2 to unity. Results pertaining to Point *B* continue to demonstrate the relatively small magnitude of u_M compared to u_e, with these two displacements remaining in phase with each other. Conversely, the motion of the two foundation platforms, described by u_e and u_s, is significantly out of phase. In this scenario, the entire external protection system functions akin to a nearly tuned mass damper for the foundation platform, effectively reducing the intensity of motion at the base of the frame structure. This action, thereby, justifies the reduced values of the performance indices at Point *B*.

Similar to Point *B*, Point *C* is located on the locus of relative minimum values (indicated by the dotted thick line) of the performance indices. For this combination of parameters, the displacements u_e and u_M remain in phase, yet the amplitude of these two displacements is comparable. The external protection system demonstrates to be effective as, in this scenario, the motion of the two foundation platforms is out-of-phase with each other. This alignment ensures effective reduction of seismic effects at the base of the frame structure.

The results obtained at Points *B* and *C*, both situated on the locus of relative minimum values of the performance indices, provide insights into the functionality of the SSSI (structure–soil–structure interaction) system. The comparison of results highlights that optimal performance is achieved when the amplitude of u_M is significantly smaller than that of the foundation platform u_e, suggesting the requirement for increased stiffness k_M. Furthermore, analysis of the performance maps for the San Jose earthquake in Figure 7, where Points *B* and *C* are located, indicates that optimal performance can be approached

asymptotically by increasing the stiffness parameter η indefinitely. This suggests that lower performance indices are achievable by employing a rigid connection between the vibrating mass and its foundation platform.
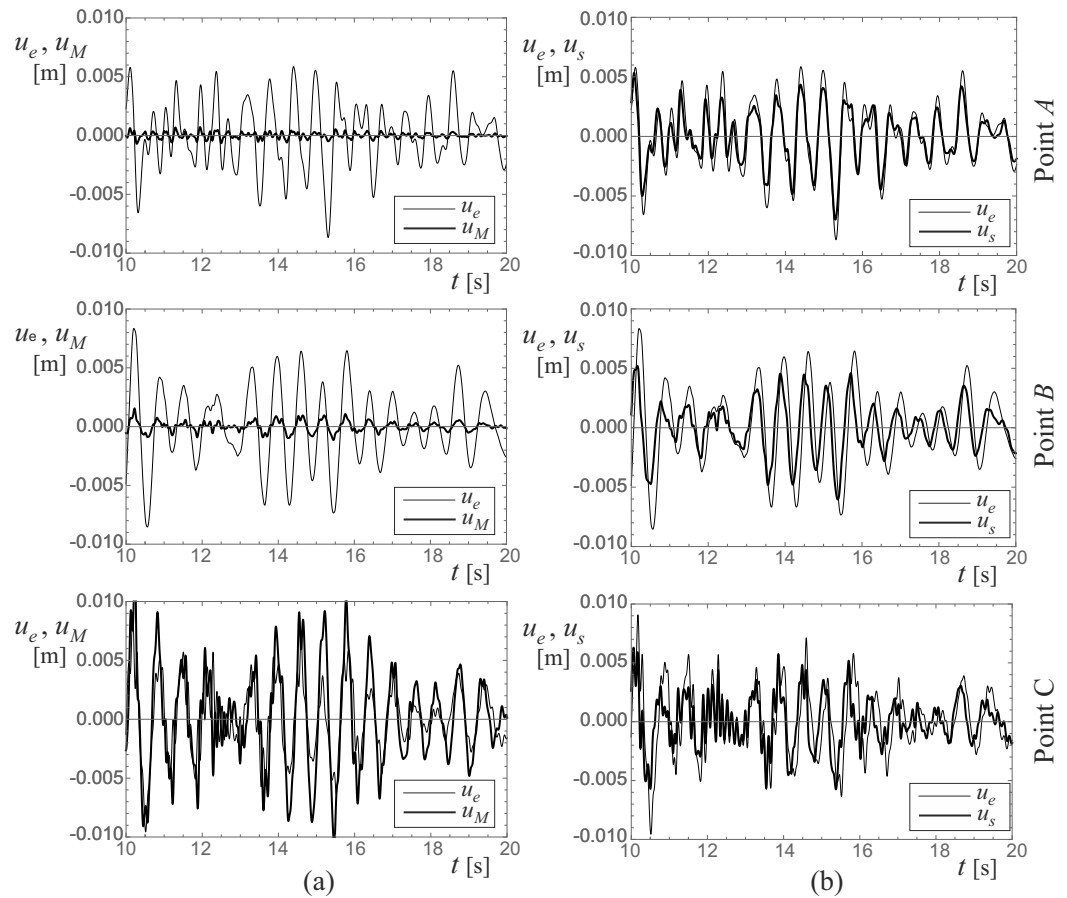

Figure 9. Time-histories of systems with characteristics labeled in points *A*, *B*, and *C* ($\eta = 4$, $\gamma = 60.0$) in Figure 7. (**a**) Displacements u_e and u_M. (**b**) Displacements u_e and u_s ($\alpha = 0.2$, $V_s = 300$ m/s, $\chi = 0.2$).

Furthermore, optimal performance of the SSSI system necessitates a specific value of the virtual mass parameter γ, which corresponds to the vertical asymptote on the locus of relative minimum values. However, achieving optimal performance typically requires a considerably high virtual mass. Given the values of the performance indexes at points *B* and *C* (Point *B*, $\alpha_1 = 0.83$, $\alpha_2 = 0.82$; Point *C*, $\alpha_1 = 0.86$, $\alpha_2 = 0.84$) and looking at the time histories of Point *C*, it can be argued that satisfactory outcomes can be achieved with a smaller virtual mass, provided that the vibrating mass M_r is allowed to move freely relative to the foundation platform.

5.4. Acceleration Maps of the SSSI System

The final analysis shifts the focus from the displacements to the accelerations. Specifically focusing on Frame 2 (refer to the second row of Tables 1 and 2), the absolute accelerations a_1 and a_2 for both stories of the 2-DOF equivalent system are computed. Subsequently, two acceleration performance indexes are introduced according to Equation (16):

$$\alpha_{a1} = \frac{\max|a_1(t)|}{\max|\tilde{a}_1(t)|}, \qquad \alpha_{a2} = \frac{\max|a_2(t)|}{\max|\tilde{a}_2(t)|}. \tag{16}$$

where $\tilde{a}_1$ and $\tilde{a}_2$ represent the absolute accelerations of the stories in the 2-degree-of-freedom (2-DOF) model corresponding to the standalone structure. The effectiveness of

the SSSI in reducing absolute accelerations improves as the values of α_{a1} and α_{a2} decrease relative to unity. The parametric investigation entails plotting the values of the acceleration performance indexes, α_{a1} and α_{a2}, in the $\eta - \gamma$ parameter space under a single earthquake record to generate acceleration performance maps. In these maps, lighter shades of gray correspond to lower values of the acceleration performance indexes.

Figure 10 shows the acceleration performance maps referring to Frame 2 under the three selected earthquakes. It is evident that the external system significantly diminishes the absolute acceleration of the first story, a_1. Moreover, the contour patterns observed in the α_{a1} maps exhibit notable distinctions from those in the α_1 maps. In contrast, the contour lines in the α_{a2} maps closely resemble those in the corresponding α_2 maps (refer to Figure 7). Nevertheless, the reduction in absolute acceleration experienced by the second story of the 2-DOF equivalent system in comparison to the standalone frame structure is notably less than the reduction observed for the first story. Despite this discrepancy, the SSSI system delivers an overall reduction in absolute acceleration across the entire frame structure.
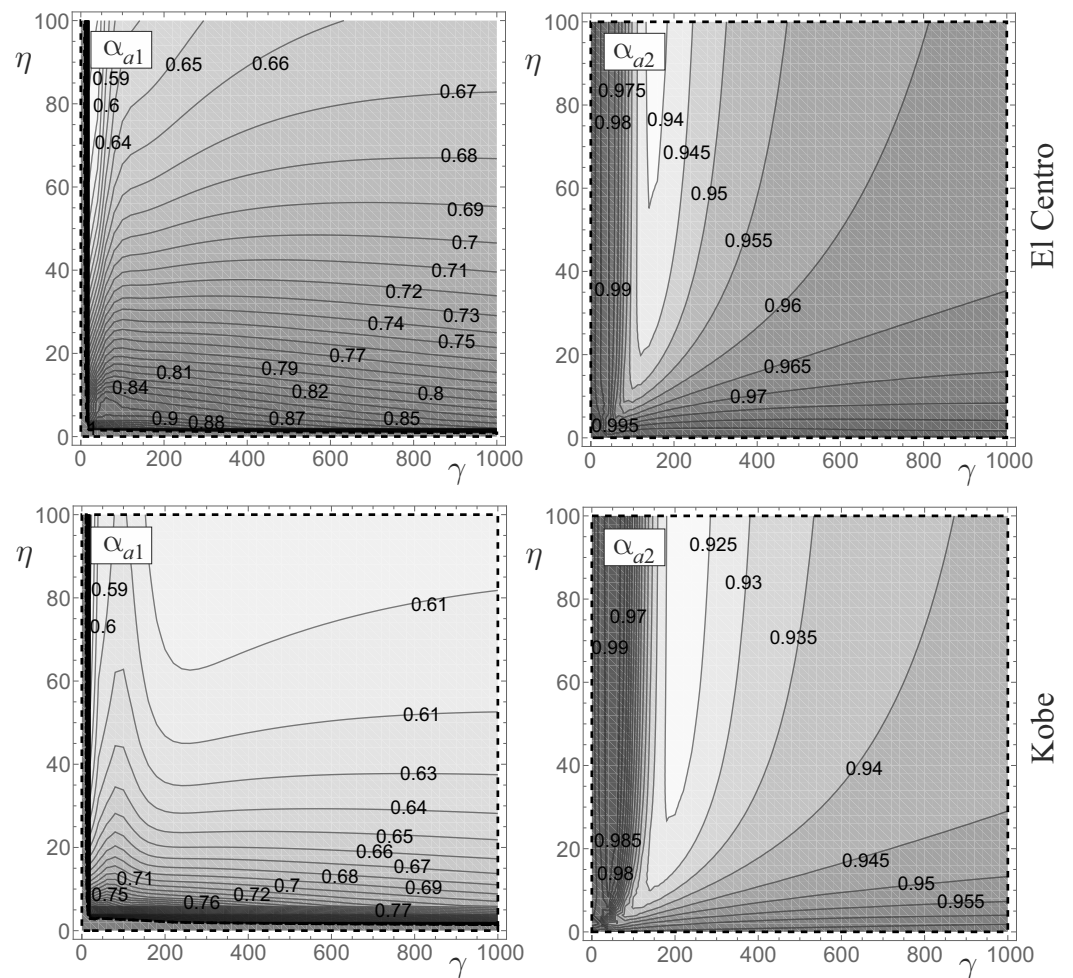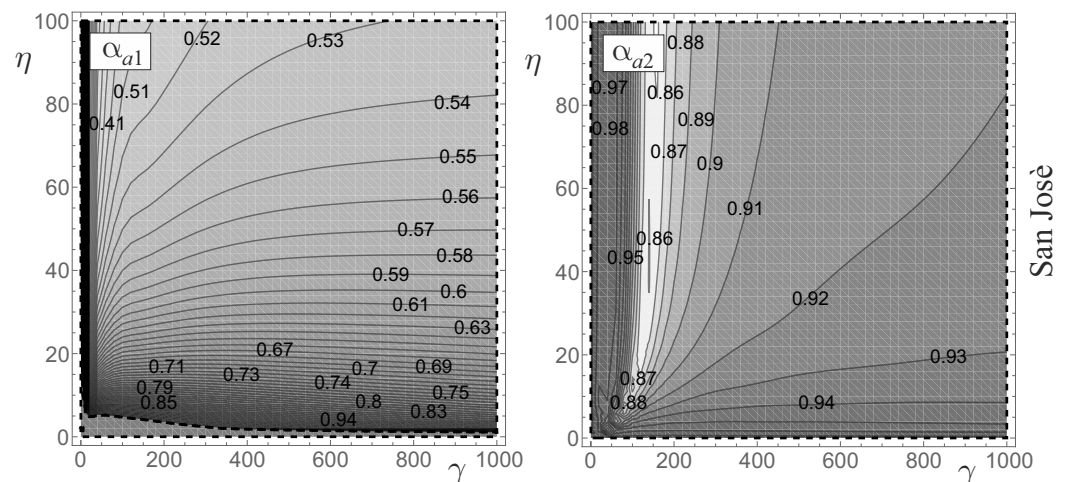

Figure 10. *Cont.*

Figure 10. Absolute acceleration maps for Frame 2 under several earthquakes ($\alpha = 0.2$, $Vs = 300$, $\chi = 0.2$).

6. Conclusions

This paper studied the reduction in the seismic response of a multi-story frame structure through the utilization of an external vibrating mass coupled with an inerter device and their interaction with the soil. The system under study comprised two identical foundation platforms. The frame structure intended for protection was considered placed on the first platform. The second platform was considered as support for a vibrating mass connected to the platform via a visco-elastic device. The studied system also included an inerter device having one terminal linked the vibrating mass and the other directly to the ground. Notably, the two platforms were not connected through any device. Both the horizontal displacements and the rotations of the platforms were considered as Lagrangian parameters, along with the horizontal displacement of the vibrating mass. Given that the multi-degree-of-freedom frame structure was represented by a 2-degree-of-freedom equivalent system, two additional Lagrangian parameters were required to fully characterize the complete system. Consequently, a seven-degrees-of-freedom mechanical model was employed to model the interacting system. The interactions between the frame structure, the soil, and the protection system were modeled using linear visco-elastic devices. The damping and stiffness of these devices were determined by utilizing established soil–structure and structure–soil–structure interaction models.

An extensive parametric analysis was conducted to investigate the performance of the system. The obtained results were organized into performance maps, which present contour plots of performance indexes specifically defined for this study. These indexes capture the ratios between the displacements and drifts of the frame structure when interacting with the soil through the vibrating mass, compared to those of the standalone frame structure. The study focused on examining the influence of parameters related to the vibrating mass and the inerter, such as the stiffness of their connection with the foundation platform and the virtual mass of the inerter device. It was observed that the system's response is significantly influenced by these parameters. Specifically, within the parameter space defined by these two factors, a region characterized by relative minimum values of both performance indexes was consistently identified. This region could be used to define preliminary optimal design parameters for the system under study.

Further results of the parametric analyses can be summarized as follows:

- The efficacy of the interaction with the external protection system (i.e., the vibrating mass and the inerter device) is enhanced by reducing the separation distance between the two foundation platforms.
- The effectiveness of the interaction with the external protection is greater in soils with low shear wave velocity (V_s).

- The performance of the interaction with the external protection system is heightened by reducing the stiffness of the soil beneath the foundation of the external protection system, such as through the implementation of a Geotechnical Seismic Isolation strategy.

In conclusion, optimal attenuation of the seismic response in the frame structure is achieved when the entire external protection system, encompassing the foundation platform, undergoes nearly counter-phase movement with the frame structure platform. This synchronization results in a diminished motion intensity at the base of the frame structure, thereby ensuring superior seismic performance of the protected structure.

References

1. Kelly, J. Base isolation: Linear theory and design. *Earthq. Spectra* **1995**, *6*, 223–244. [CrossRef]
2. Den Hartog, J.P. *Mechanical Vibrations*, 4th ed.; McGraw-Hill: New York, NY, USA, 1956.
3. Tsai, H.H. The effect of tuned-mass dampers on the seismic response of base-isolated structures. *Int. J. Solid Struct.* **1995**, *32*, 1195–1210. [CrossRef]
4. Taniguchi, T.; Kiureghian, A.D.; Melkumyan, M. Effect of tuned mass damper on displacement demand of base-isolated structures. *Eng. Struct.* **2008**, *30*, 3478–3488. [CrossRef]
5. De Domenico, D.; Impollonia, N.; Ricciardi, G. Soil-dependent optimum design of a new passive vibration control system combining seismic base isolation with tuned inerter damper. *Soil Dyn. Earthq. Eng.* **2018**, *105*, 37–53. [CrossRef]
6. Giaralis, A.; Taflanidis, A. Optimal tuned mass-damper-inerter (TMDI) design for seismically excited MDOF structures with model uncertainties based on reliability criteria. *Struct. Control Health Monit.* **2018**, *25*, e2082. [CrossRef]
7. Pietrosanti, D.; De Angelis, M.; Basili, M. Optimal design and performance evaluation of systems with Tuned Mass Damper Inerter (TMDI). *Earthq. Eng. Struct. Dyn.* **2017**, *46*, 1367–1388. [CrossRef]
8. Pietrosanti, D.; De Angelis, M.; Basili, M. A generalized 2-DOF model for optimal design of MDOF structures controlled by Tuned Mass Damper Inerter (TMDI). *Int. J. Mech. Sci.* **2020**, *185*, 105849. [CrossRef]
9. Di Egidio, A.; Contento, A. Seismic Benefits from Coupling Frame Structures with a Hysteretic Mass Damper Inerter. *Appl. Sci.* **2023**, *13*, 5017. [CrossRef]
10. Di Egidio, A.; Pagliaro, S.; Contento, A. Seismic benefits of deformable connections between a frame structure and an external structure with inerter. *Eng. Struct.* **2022**, *256*, 113025. [CrossRef]
11. Vicencio, F.; Alexander, N.A.; Saavedra Flores, E.I. A State-of-the-Art review on Structure-Soil-Structure interaction (SSSI) and Site-City interactions (SCI). *Structures* **2023**, *56*, 105002. [CrossRef]
12. Cacciola, P.; Espinosa, M.G.; Tombari, A. Vibration control of piled-structures through structure-soil-structure-interaction. *Soil Dyn. Earthq. Eng.* **2015**, *77*, 47–57. [CrossRef]
13. Cacciola, P.; Banjanaca, N.; Tombari, A. Vibration Control of an existing building through the Vibrating Barrier. *Procedia Eng.* **2017**, *199*, 1598–1603. [CrossRef]
14. Cacciola, P.; Tombari, A.; Giaralis, A. An inerter-equipped vibrating barrier for noninvasive motion control of seismically excited structures. *Struct. Control Health Monit.* **2020**, *27*, e2474. [CrossRef]
15. Makris, N.; Kampas, G. Seismic Protection of Structures with Supplemental Rotational Inertia. *J. Eng. Mech.* **2016**, *142*, 04016089. [CrossRef]
16. Thiers-Moggia, R.; Málaga-Chuquitaype, C. Seismic protection of rocking structures with inerters. *Earthq. Eng. Struct. Dyn.* **2018**, *48*, 528–547. [CrossRef]
17. Cacciola, P.; Tombari, A.; Giaralis, A. A vibrating barrier with grounded inerter for non- invasive seismic protection of existing structures. In Proceedings of the 16th European Conference on Earthquake Engineering—16ECEE, Thessaloniki, Greece, 18–21 June 2018.
18. Mulliken, J.S.; Discrete Models for Foundation–Soil–Foundation Interaction in Time Domain. Master's Thesis, University of South Carolina, Columbia, SC, USA, 1994.

19. Mulliken, J.S.; Karabalis, D.L. Discrete model for foundation–soil–foundation interaction. *Soil Dyn. Earthq. Eng.* **1995**, *VII*, 501–508.
20. Mulliken, J.S.; Karabalis, D.L. Discrete Model for Dynamic Through-The-Soil Coupling of 3-D Foundations and Structures. *Earthq. Eng. Struct. Dyn.* **1998**, *27*, 687–710. [CrossRef]
21. Fabrizio, C.; de Leo, A.; Di Egidio, A. Tuned mass damper and base isolation: A unitary approach for the seismic protection of conventional frame structures. *J. Eng. Mech.* **2019**, *145*, 04019011. [CrossRef]
22. Pagliaro, S.; Di Egidio, A. Archetype dynamically equivalent 3-d.o.f. model to evaluate seismic performances of intermediate discontinuity in frame structures. *J. Eng. Mech.* **2022**, *148*, 04022004. [CrossRef]
23. Tsang, H. Analytical design models for geotechnical seismic isolation systems. *Bull. Earthq. Eng.* **2023**, *21*, 3881–3904. [CrossRef]
24. Tsang, H.; Pitilakis, K. Mechanism of geotechnical seismic isolation system: Analytical modeling. *Soil Dyn. Earthq. Eng.* **2019**, *122*, 171–184. [CrossRef]
25. Available online: https://www.strongmotioncenter.org/ (accessed on 15 January 2024).